



Deposited via The University of Leeds.

White Rose Research Online URL for this paper:

<https://eprints.whiterose.ac.uk/id/eprint/95856/>

Version: Accepted Version

---

**Article:**

Howell, FW, Haywood, AM, Dowsett, HJ et al. (2016) Sensitivity of Pliocene Arctic climate to orbital forcing, atmospheric CO<sub>2</sub> and sea ice albedo parameterisation. *Earth and Planetary Science Letters*, 441. pp. 133-142. ISSN: 0012-821X

<https://doi.org/10.1016/j.epsl.2016.02.036>

---

© 2016, Elsevier. Licensed under the Creative Commons Attribution-NonCommercial-NoDerivatives 4.0 International <http://creativecommons.org/licenses/by-nc-nd/4.0/>

**Reuse**

Items deposited in White Rose Research Online are protected by copyright, with all rights reserved unless indicated otherwise. They may be downloaded and/or printed for private study, or other acts as permitted by national copyright laws. The publisher or other rights holders may allow further reproduction and re-use of the full text version. This is indicated by the licence information on the White Rose Research Online record for the item.

**Takedown**

If you consider content in White Rose Research Online to be in breach of UK law, please notify us by emailing [eprints@whiterose.ac.uk](mailto:eprints@whiterose.ac.uk) including the URL of the record and the reason for the withdrawal request.

# Sensitivity of Pliocene Arctic climate to orbital forcing, atmospheric CO<sub>2</sub> and sea ice albedo parameterisation

Fergus W. Howell<sup>a,\*</sup>, Alan M. Haywood<sup>a</sup>, Harry J. Dowsett<sup>b</sup>, Steven J. Pickering<sup>a</sup>

<sup>a</sup>*School of Earth and Environment, University of Leeds, Woodhouse Lane, Leeds, LS2 9JT, UK*

<sup>b</sup>*Eastern Geology and Paleoclimate Science Center, US Geological Survey, 12201 Sunrise Valley Drive, Reston, Virginia, 20192, USA*

---

## 1 Abstract

2 General circulation model (GCM) simulations of the mid-Pliocene Warm Period (mPWP, 3.264  
3 to 3.025 Myr ago) do not reproduce the magnitude of Northern Hemisphere high latitude surface  
4 air and sea surface temperature (SAT and SST) warming that proxy data indicates. There is also  
5 large uncertainty regarding the state of sea ice cover in the mPWP. Evidence for both perennial and  
6 seasonal mPWP Arctic sea ice is found through analyses of marine sediments, whilst in a multi-  
7 model ensemble of mPWP climate simulations, half of the ensemble simulated ice-free summer  
8 Arctic conditions. Given the strong influence that sea ice exerts on high latitude temperatures, an  
9 enhanced understanding of the nature of mPWP Arctic sea ice would be highly beneficial.

10 Using the HadCM3 GCM, this paper explores the impact of various combinations of potential  
11 mPWP orbital forcing, atmospheric CO<sub>2</sub> concentrations and minimum sea ice albedo on sea ice  
12 extent and high latitude warming. The focus is on the Northern Hemisphere, due to availability  
13 of proxy data, and the large data-model discrepancies in this region. Changes in orbital forcings  
14 are demonstrated to be sufficient to alter the Arctic sea ice simulated by HadCM3 from perennial  
15 to seasonal. However, this occurs only when atmospheric CO<sub>2</sub> concentrations exceed 300 ppm.  
16 Reduction of the minimum sea ice albedo from 0.5 to 0.2 is also sufficient to simulate seasonal sea  
17 ice, with any of the combinations of atmospheric CO<sub>2</sub> and orbital forcing. Compared to a mPWP  
18 control simulation, monthly mean increases north of 60°N of up to 4.2°C (SST) and 9.8°C (SAT)  
19 are simulated.

20 With varying CO<sub>2</sub>, orbit and sea ice albedo values we are able to reproduce proxy temperature  
21 records that lean towards modest levels of high latitude warming, but other proxy data showing  
22 greater warming remain beyond the reach of our model. This highlights the importance of addi-  
23 tional proxy records at high latitudes and ongoing efforts to compare proxy signals between sites.

## 24 *Keywords:*

25 palaeoclimate, Pliocene, climate model, sea ice, orbital variability, CO<sub>2</sub>

---

\*Corresponding author

*Email address:* eefwh@leeds.ac.uk (Fergus W. Howell)

## 26 1. Introduction

27 The mid-Pliocene Warm Period (mPWP, 3.264 to 3.025 Myr ago (Dowsett et al., 2010)) is  
28 widely characterised as a period of sustained warmth in Earth's history (e.g. Haywood and Valdes  
29 (2004); Haywood et al. (2013)), with mean annual temperatures thought to be 2-3°C higher than the  
30 pre-industrial era. Estimates of mid-Pliocene pCO<sub>2</sub> have typically been within the range of 365-415  
31 ppm (Pagani et al., 2010; Seki et al., 2010), but other studies have suggested that it may have been  
32 lower, around 270-300 ppm (e.g. Zhang et al. (2013); Badger et al. (2013)). GCM simulations of  
33 the mPWP have not reproduced the magnitude of high-latitude warming of sea surface and surface  
34 air temperatures (SSTs and SATs) indicated by proxy data (e.g. Dowsett et al. (2011); Salzmann  
35 et al. (2013)). A detailed understanding of forcings which have a strong effect on high latitude  
36 climates is therefore important, as their representation in models may have a strong impact on the  
37 simulated climates of the past, present and future.

38 The representation of sea ice in models is one such example. Sea ice can enhance perturbations  
39 to the climate via feedback processes such as albedo, in addition to acting as an insulator between  
40 the ocean and the atmosphere (Kellogg, 1975; Maykut, 1978; Curry et al., 1995). Previous studies  
41 have attempted to reduce the discrepancy between mid-Pliocene high latitude temperature estimates  
42 derived from proxy data and model simulated temperatures through reduced sea ice cover. This  
43 has been done by artificially removing it year-round in an atmosphere-only simulation (Ballantyne  
44 et al., 2013), or by changes to the parameterisation of some sea ice processes (Howell et al., 2014).

45 Understanding of the state of Arctic sea ice from proxy data in the mid-Pliocene remains lim-  
46 ited. Based on the presence of iron grains in marine sediments (located at 87.5°N, 138.3°W), Darby  
47 (2008) concludes that the Arctic has had perennial sea ice for the past 14 million years. Analysis  
48 of IP<sub>25</sub>, a sea ice proxy biomarker (Belt et al., 2007; Brown et al., 2014), in two cores (located at  
49 80.2°N, 6.4°E and 80.3°N, 8.1°E) by Knies et al. (2014) shows that the mid-Pliocene minimum sea  
50 ice margin was located to the north of these two sites. Cronin et al. (1993), Moran et al. (2006) and  
51 Polyak et al. (2010) show evidence from ostracode assemblages and ice rafted debris that appear  
52 to suggest that the mid-Pliocene Arctic sea ice cover was seasonal in nature.

53 The Pliocene Modelling Intercomparison Project (PlioMIP) has compared the output of the  
54 simulation of the mPWP by GCMs from eight different modelling groups (Haywood et al., 2013).  
55 Howell et al. (2015) showed that variability in the ensemble simulation of mid-Pliocene Arctic sea  
56 ice is high in the summer months, where four of the models simulate ice-free summers, and the  
57 other four, including HadCM3, maintain at least some sea ice coverage year-round.

58 Model simulations of the mPWP, such as those performed for PlioMIP, typically represent  
59 the mid-Pliocene through a fixed atmospheric CO<sub>2</sub> concentration, usually ~ 400 ppm, and orbital  
60 configuration typically identical to modern (Haywood et al., 2011). However, the mPWP time slab  
61 is ~ 240,000 years long, across which there may have been variations in pCO<sub>2</sub>, as well as changes  
62 in orbital forcing, which will have affected the state of the Arctic sea ice cover.

63 This paper focuses on two main issues. It explores the sensitivity of modelled mid-Pliocene  
64 Arctic sea ice in HadCM3 to variations in orbital configuration, atmospheric CO<sub>2</sub> concentration and  
65 sea ice albedo parameterisation, in isolation as well as in combinations of these factors. In addition,

66 through focusing on those simulations where there is the most extreme reductions in sea ice, this  
67 paper investigates the extent to which such large changes can influence the outcomes of data-model  
68 comparison, and if they are capable of bringing model and data results into closer agreement.

## 69 **2. Methods**

### 70 *2.1. Model description*

71 The simulations carried out in this paper were run using HadCM3 (Hadley Centre Coupled  
72 Climate Model version 3), a coupled atmosphere-ocean GCM from the UK Met Office. The model  
73 incorporates sea ice and vegetation components in addition to the atmosphere and ocean compo-  
74 nents (Gordon et al., 2000).

75 The ocean component contains 20 vertical levels, and has a horizontal resolution of  $1.25^\circ \times$   
76  $1.25^\circ$ , which gives a grid box at the equator of approximately  $139 \text{ km} \times 139 \text{ km}$ . Vertical levels are  
77 distributed to allow greater resolution closer to the surface (Gordon et al., 2000). The atmosphere  
78 component of the model contains 19 vertical levels with a horizontal resolution of  $2.5^\circ \times 3.75^\circ$   
79 (latitude  $\times$  longitude), giving six ocean boxes for every atmosphere grid box. Schemes incorporated  
80 in the atmosphere component include a radiation scheme representing effects of minor trace gases  
81 (Edwards and Slingo, 1996), a land surface scheme capable of representing the effects of soil  
82 moisture melting and freezing (Cox et al., 1999) and a gravity wave drag parameterisation (Gregory  
83 et al., 1998).

84 Parameterisations of ice drift and leads, combined with a basic thermodynamic scheme, are  
85 the basis of the sea ice model in HadCM3 (Cattle and Crossley, 1995; Gordon et al., 2000). The  
86 thermodynamic scheme is based on the zero-layer model from Semtner (1976), developed from  
87 the one-dimensional sea ice model described in Maykut and Untersteiner (1971). Ice dynamics are  
88 based on parameterisations described by Bryan (1969). Sea ice advection is derived from the mean  
89 current speeds in the top 100 m of the ocean, which are based on windstress in HadCM3 (Gordon  
90 et al., 2000). The parameterisation of sea ice concentration is based on Hibler (1979). For SATs  
91 between  $-10^\circ\text{C}$  and  $0^\circ\text{C}$ , sea ice albedo is a linear function of the temperature. Albedo is 0.8 at  
92  $-10^\circ\text{C}$  and colder, and 0.5 at  $0^\circ\text{C}$ . Salinity of sea ice is constant, at  $0.6\text{‰}$ .

### 93 *2.2. Experimental design*

94 Including the control, thirty simulations of the mid-Pliocene are run. These comprise all combi-  
95 nations of five orbital configurations, three concentrations of atmospheric  $\text{CO}_2$ , and two minimum  
96 sea ice albedo values. These are summarised in Table 1, which also describes the notation used  
97 to identify individual simulations. In addition to the mid-Pliocene simulations, a simulation with  
98 pre-industrial boundary conditions was also run. Each simulation was run for 500 years, spun off  
99 from the same 500 year control run, which was sufficient to ensure all simulations reached an equi-  
100 librium state. Climatological averages are based on the last 30 years, and the boundary conditions  
101 used are derived from PRISM3D, a reconstruction of mPWP sea surface and deep ocean tempera-  
102 tures, in addition to sea level, topography, vegetation and ice sheet reconstructions (Dowsett et al.,  
103 2010), following the PlioMIP alternate experimental design outlined in Haywood et al. (2011).

### 104 2.2.1. *Orbital configurations*

105 In addition to the control (orbit identical to modern), simulations of the mPWP were run with  
106 four alternative orbital configurations. These were selected to test the sensitivity of simulated Arctic  
107 sea ice in the mPWP to increased insolation at different times of the year. The four alternative orbits  
108 selected were those that, according to the astronomical solution of Laskar et al. (2004), gave the  
109 greatest insolation at 65°N in the mPWP during January, March, July and September. January and  
110 July were selected due to being the middle months of the traditional definitions of winter (DJF)  
111 and summer (JJA) respectively. March and September were selected as Arctic sea ice reaches  
112 its maximum and minimum extents respectively in these months. Eccentricity, precession and  
113 obliquity values for each orbital configuration are summarised in Table 1.

### 114 2.2.2. *Atmospheric CO<sub>2</sub> concentrations*

115 Atmospheric CO<sub>2</sub> concentrations of 300 ppm and 500 ppm are used, in addition to the control  
116 level of 400 ppm. Whilst some studies have suggested that 300 ppm is a plausible pCO<sub>2</sub> value  
117 for the mPWP, or at least for some part of the period (e.g. (Zhang et al., 2013; Badger et al.,  
118 2013)), 500 ppm is greater than the maximum values that have normally been suggested for the  
119 mid-Pliocene. The 500 ppm solutions are intended to provide a guide to the sensitivity of the  
120 Arctic sea ice to changes in pCO<sub>2</sub>, and the state of the Arctic climate under extreme forcings to the  
121 sea ice, rather than a simulation of a mid-Pliocene climate that is likely to have necessarily existed.  
122 CO<sub>2</sub> is only one greenhouse gas, and others such as CH<sub>4</sub> have traditionally been omitted in mid-  
123 Pliocene experiments. A pCO<sub>2</sub> value of 500 ppm could therefore provide the overall increase in  
124 radiative forcing as a result from CO<sub>2</sub> and other greenhouse gases.

### 125 2.2.3. *Minimum sea ice albedo*

126 Recent observations have demonstrated that sea ice albedos are generally lower on seasonal  
127 sea ice in comparison to multi-year sea ice (Perovich and Polashenski, 2012; Riihela et al., 2013).  
128 Howell et al. (2014) suggested that the standard parameterisation of sea ice albedo in HadCM3,  
129 with a fixed lower limit of 0.5, may not be appropriate for the mPWP. With a warmer than present  
130 climate the Arctic sea ice cover is likely to have consisted of a greater proportion of seasonal sea  
131 ice compared to present day. Howell et al. (2014) used parameterisations with alternative lower  
132 limits of 0.2, 0.3 and 0.4. The lowest limit of 0.2 is used in the ensemble in this study, along with  
133 the control lower limit of 0.5.

## 134 2.3. *Data analysis techniques*

### 135 2.3.1. *Data-model comparison*

136 This paper uses the same methods as Howell et al. (2014) for the data-model comparison.  
137 Proxy data temperature estimates for SATs are based on palaeobotanical data (Salzmann et al.,  
138 2008, 2013) and for SSTs from planktonic foraminiferal assemblages, and Mg/Ca and alkenone  
139 paleothermometry (Dowsett et al., 2010, 2013; Schreck et al., 2013; Knies et al., 2014).

140 Data sites north of 60°N provide the focus for this paper, as this is where the significant warm-  
141 ing is observed in model simulations. Howell et al. (2014) focuses on just six data sites, three

142 marine and three terrestrial, as temperature changes are small at all other sites. This paper extends  
143 the focus of the DMC to all data sites north of 60°N where the proxy data temperature estimate  
144 exceeds the mean annual temperature from the control simulation. Locations of the sites are shown  
145 in Figure 1.

146 In addition to the sites used in Howell et al. (2014), mid-Pliocene Arctic SST estimates from  
147 Schreck et al. (2013) and Knies et al. (2014), are included. The SST estimate for ODP 911 from  
148 Robinson (2009) is not included in this paper, as a newer age model presented by Mattingdal et al.  
149 (2014) put the samples outside the mPWP. The terrestrial site Ocean Point (Nelson and Carter,  
150 1985) is not included in this paper as age estimates for the site are 2.7 – 2.6 Myr ago, and so is  
151 outside the mPWP. A recent mid-Pliocene SAT estimate from Pound et al. (2015) is added to the  
152 terrestrial data-model comparison.

153 The data-model comparison will focus on the difference between the proxy data estimates and  
154 the highest mean annual temperature in the ensemble at each data site. In addition to the mean  
155 annual temperature, the highest monthly temperature increase in the ensemble at each data site will  
156 be shown.

### 157 2.3.2. *Energy balance analysis*

158 This paper uses the methods set out in Hill et al. (2014) to determine the breakdown of contri-  
159 bution to high latitude SAT changes in selected simulations, enabling an analysis of the differences  
160 in patterns of temperature and sea ice changes resulting from the different forcing changes.

## 161 3. Results

### 162 3.1. *Sea Ice*

#### 163 3.1.1. *Sea ice extent*

164 23 of the simulations produce a lower mean annual sea ice extent than the control simulation  
165 (Mod\_400\_0.5,  $10.61 \times 10^6$  km<sup>2</sup>), with 6 producing higher mean annual extents (all 5 simulations  
166 with 300 ppm pCO<sub>2</sub> and standard albedo, and Mar\_400\_0.5). The annual sea ice extent cycles for  
167 each of the 30 simulations are displayed in Figure 2.

168 The effects of changing only the orbital configurations from the PlioMIP experimental design  
169 are shown in Figure 2(c), which includes the control simulation, Mod\_400\_0.5. Compared to the  
170 control, the mean annual extent is higher in Mar\_400\_0.5, and lower for the other three orbits.  
171 Of these, Jul\_400\_0.5 simulates the smallest mean annual extent ( $8.92 \times 10^6$  km<sup>2</sup>, a decrease of  
172 15.90% compared to the control).

173 The September sea ice extent minimum simulated by Jul\_400\_0.5 (Figure 2(c)) is  $0.37 \times 10^6$   
174 km<sup>2</sup>, which meets the criteria for ‘sea ice free’ conditions of less than  $10^6$  km<sup>2</sup> (e.g. Wang and  
175 Overland (2009)). This demonstrates that a change in orbital configuration only from the control is  
176 sufficient to simulate sea ice free conditions in the mid-Pliocene (using the HadCM3 model).

177 A striking feature of Figure 2(c) is the difference in summer sea ice in the Jul\_400\_0.5 sim-  
178 ulation compared to the other orbital configurations. The Jul\_400\_0.5 summer sea ice extent is  
179  $2.34 \times 10^6$  km<sup>2</sup> (70.0%) lower than the control summer sea ice extent, and in September measures

Table 1: Combinations of orbital configuration (with eccentricity, precession and obliquity values), pCO<sub>2</sub> and minimum sea ice albedo of the 30 simulations. The control simulation is highlighted in bold.

| Experiment name    | Orbital Equivalent (kyr BP) | Eccentricity/ Precession/ Obliquity | Atmospheric CO <sub>2</sub> concentration (ppmv) | Minimum albedo |
|--------------------|-----------------------------|-------------------------------------|--|----------------|
| Mod_300_0.5        |                             |                                     | 300  | 0.5            |
| <b>Mod_400_0.5</b> |                             | 0.016702                            | 400  | 0.5            |
| Mod_500_0.5        | Modern                      | 0.01628                             | 500  | 0.5            |
| Mod_300_0.2        |                             | 23.439                              | 300  | 0.2            |
| Mod_400_0.2        |                             |                                     | 400  | 0.2            |
| Mod_500_0.2        |                             |                                     | 500  | 0.2            |
| Jan_300_0.5        |                             |                                     | 300  | 0.5            |
| Jan_400_0.5        |                             | 0.053487                            | 400  | 0.5            |
| Jan_500_0.5        | 3057                        | -0.02318                            | 500  | 0.5            |
| Jan_300_0.2        |                             | 22.914                              | 300  | 0.2            |
| Jan_400_0.2        |                             |                                     | 400  | 0.2            |
| Jan_500_0.2        |                             |                                     | 500  | 0.2            |
| Mar_300_0.5        |                             |                                     | 300  | 0.5            |
| Mar_400_0.5        |                             | 0.040574                            | 400  | 0.5            |
| Mar_500_0.5        | 3140                        | 0.02343                             | 500  | 0.5            |
| Mar_300_0.2        |                             | 22.719                              | 300  | 0.2            |
| Mar_400_0.2        |                             |                                     | 400  | 0.2            |
| Mar_500_0.2        |                             |                                     | 500  | 0.2            |
| Jul_300_0.5        |                             |                                     | 300  | 0.5            |
| Jul_400_0.5        |                             | 0.051086                            | 400  | 0.5            |
| Jul_500_0.5        | 3037                        | -0.04239                            | 500  | 0.5            |
| Jul_300_0.2        |                             | 23.642                              | 300  | 0.2            |
| Jul_400_0.2        |                             |                                     | 400  | 0.2            |
| Jul_500_0.2        |                             |                                     | 500  | 0.2            |
| Sep_300_0.5        |                             |                                     | 300  | 0.5            |
| Sep_400_0.5        |                             | 0.054281                            | 400  | 0.5            |
| Sep_500_0.5        | 3053                        | 0.03551                             | 500  | 0.5            |
| Sep_300_0.2        |                             | 22.947                              | 300  | 0.2            |
| Sep_400_0.2        |                             |                                     | 400  | 0.2            |
| Sep_500_0.2        |                             |                                     | 500  | 0.2            |

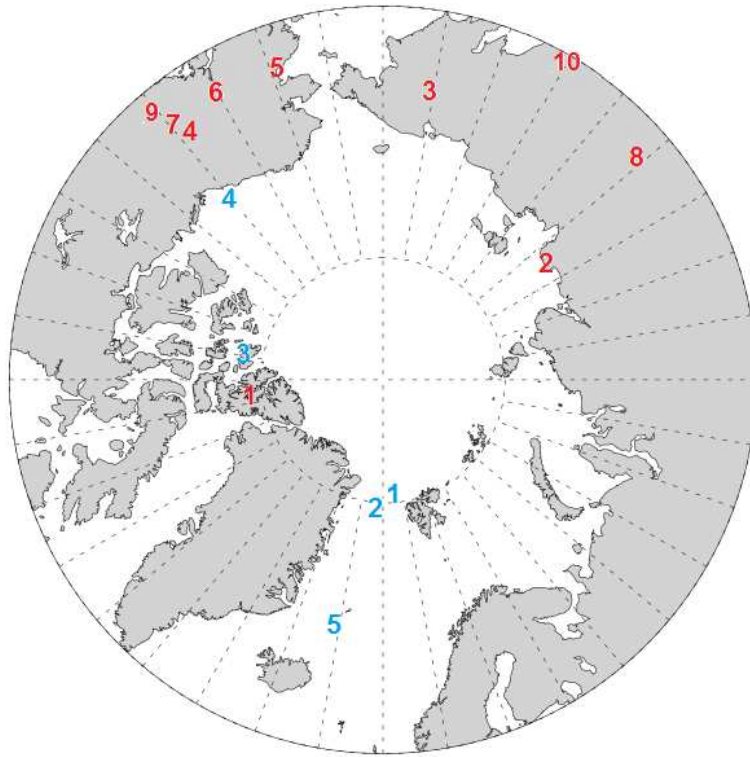


Figure 1: Location of marine (blue) and terrestrial (red) data sites. Marine data sites: 1. ODP 910C, 2. ODP 909C, 3. Meighen Island, 4. Colvillian, 5. ODP 907A. Terrestrial data sites: 1. Beaver Pond, 2. Lena River, 3. Lake El'gygytyn, 4. Alaska Circle, 5. Blizkiy, 6. Nenana Valley, 7. Lost Chicken Mine, 8. Delyankir, 9. Bonanza Creek, 10. Magadan District.

180 just  $0.37 \times 10^6 \text{ km}^2$ , classified as 'sea ice-free' as it is less than  $10^6 \text{ km}^2$  (e.g. Wang and Over-  
 181 land (2009)). This demonstrates the importance of the orbital configuration on the simulation of  
 182 mid-Pliocene Arctic sea ice.

183 Raising the atmospheric  $\text{CO}_2$  levels to 500 ppm (Figure 2(a, b)) results in a decline in sea ice  
 184 in every month for all five orbits. In each simulation, the largest reduction occurs in November.  
 185 From August to September, both the Jan\_500\_0.5 and Jul\_500\_0.5 simulations produce a sea ice  
 186 free Arctic, but the extent in the Mod\_500\_0.5 simulation does not fall below  $1.62 \times 10^6 \text{ km}^2$ .  
 187 Reduction of the atmospheric  $\text{CO}_2$  concentration to 300 ppm (Figure 2(e, f)) has the effect of an  
 188 increase in sea ice extent in every month, with none of the simulations in this scenario producing  
 189 sea ice-free months.

190 Reducing minimum albedo to 0.2 also causes a decrease in sea ice extent in each month of  
 191 every orbital simulation, compared to the same orbit under standard conditions. All five simulations  
 192 produce no sea ice from August to October, with the Jul\_400\_0.2 simulation also producing no sea

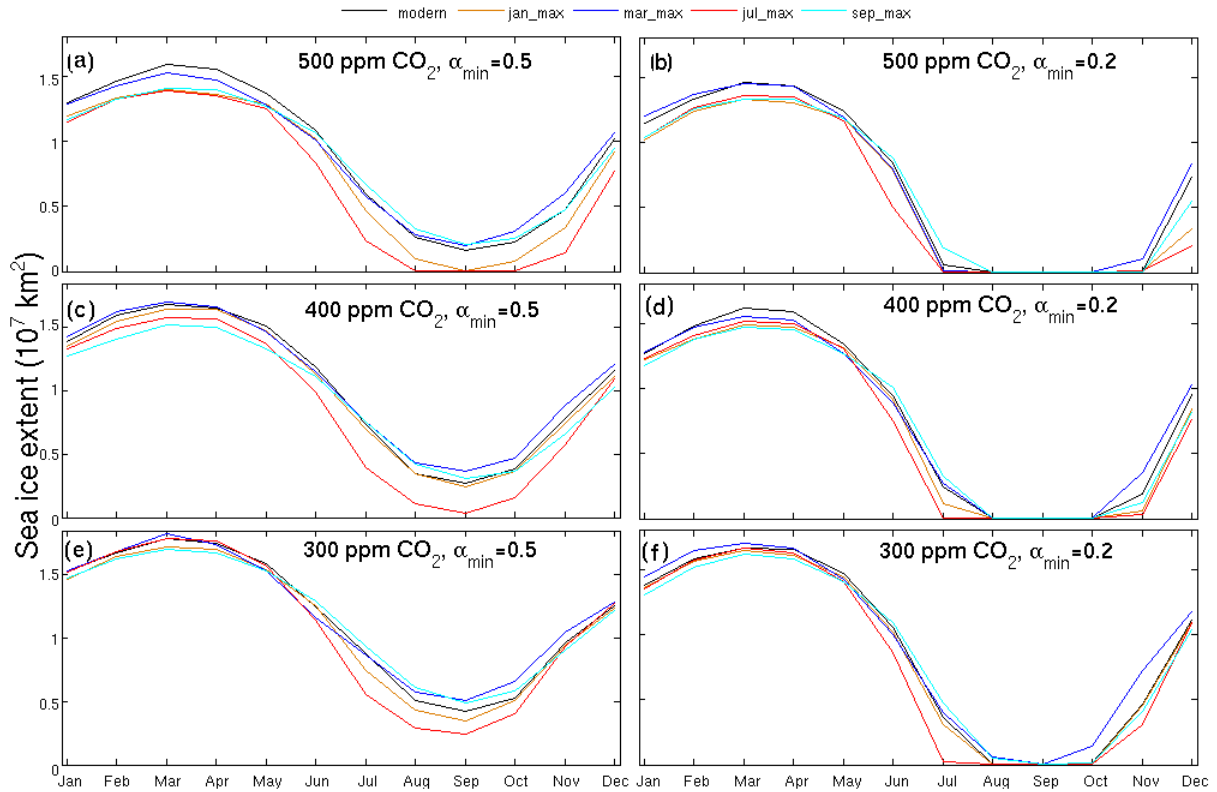


Figure 2: Annual sea ice extent ( $10^7 \text{ km}^2$ ) cycle for all 30 ensemble members. Each panel shows the five orbital simulations with the same  $\text{pCO}_2$  and minimum albedo combinations. The only difference between simulations in any given panel is the orbital configuration used.

193 ice in July. With atmospheric  $\text{CO}_2$  levels at 300 ppm and reduced minimum albedo, all simulations  
 194 produce months with an ice-free Arctic, but have a more rapid sea ice growth in November and  
 195 December compared to the 400 ppm simulation. Increasing the atmospheric  $\text{CO}_2$  to 500 ppm with  
 196 reduced minimum albedo results in a longer ice-free Arctic period in most of the simulations, and  
 197 a slower recovery in November and December.

198 The mean annual change in sea ice extent is  $2.11 \times 10^6 \text{ km}^2$  (19.9%). The main driver of this  
 199 is summer sea ice extent, which sees a mean change of  $2.35 \times 10^6 \text{ km}^2$  (69.4%), contrasting to a  
 200 mean winter change of just  $1.46 \times 10^6 \text{ km}^2$  (8.9%).

### 201 3.1.2. Sea ice thickness

202 23 simulations produce a thinner mean annual sea ice cover (north of  $80^\circ\text{N}$ ) in comparison to  
 203 the control simulation (Mod\_400\_0.5), the same number of simulations that showed a decline in  
 204 mean annual extent. Figure 3 shows mean annual thickness anomalies for eight of the simulations

205 (chosen to display the range of different changes in sea ice thickness, SAT (Figure 4) and SST  
 206 (Figure 5), plots for all simulations shown in supplementary information). In all simulations, the  
 207 change in mean annual thickness is the same sign as the change in mean annual extent, with two  
 208 exceptions (Sep\_400\_0.5 simulation simulates a thicker ice cover, despite also simulating a reduced  
 209 extent, and Jul\_300\_0.5 simulates thinner than control sea ice, in addition to a greater extent).

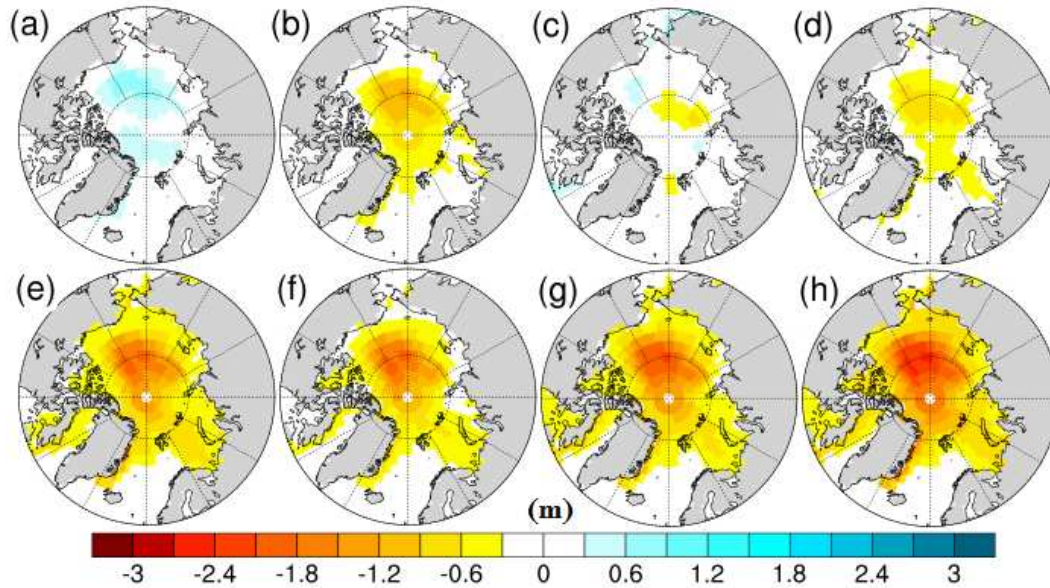


Figure 3: Mean annual sea ice thickness (m) anomaly (alternative minus control) for simulations: (a) Mar\_400\_0.5 (b) Jul\_400\_0.5 (c) Jul\_300\_0.5 (d) Mod\_500\_0.5 (e) Jul\_500\_0.5 (f) Mod\_400\_0.2 (g) Mod\_500\_0.2 (h) Jul\_500\_0.2. Control simulation is Mod\_400\_0.5.

210 The change in mean annual sea ice thickness north of 80°N across the ensemble is 0.73 m  
 211 (34.3%). The mean change in winter is 0.71 m (20.1%), and 0.65 m (72.6%) in summer. The  
 212 seasonal changes in thickness are far closer in value in comparison to the seasonal changes in  
 213 extent, although the change of 0.65 m in summer represents a proportionally much greater change  
 214 from the control than the winter change of 0.71 m.

215 The simulations with increased atmospheric CO<sub>2</sub> produced less extensive, but thicker winter  
 216 sea ice in comparison to the simulations with reduced minimum albedo. The mean sea ice thickness  
 217 north of 80°N thins by an average of 0.54 m in comparison to the control in the increased pCO<sub>2</sub>  
 218 simulations, whilst the decreased minimum albedo simulations show an average thinning of 0.97  
 219 m.

220 3.2. Temperature changes

221 3.2.1. Annual and seasonal changes

222 The large reduction in sea ice seen in many of the simulations has substantial effects on the  
223 modelled SATs and SSTs. Feedback processes mean that reduced sea ice will likely be both a  
224 cause of and result of increased temperatures. All but one simulation where the mean annual sea  
225 ice extent was reduced in comparison to the control have increases in the mean annual SATs and  
226 SSTs north of 60°N. The exception is Mar\_300\_0.2 simulation, where the mean annual SAT and  
227 SST are reduced, in comparison to the control, by 0.2°C and 0.03°C respectively. Figures 4 and 5  
228 show mean annual SAT and SST anomalies for eight of the ensemble members, whilst Figures 6  
229 and 7 show SAT and SST seasonal anomalies for the Jul\_500\_0.2 simulation.

230 Changes in SAT are on average greater than changes in SST. For example, as a result of increas-  
231 ing pCO<sub>2</sub> to 500 ppm, the mean annual increase in SST north of 60°N compared to the control is  
232 0.9°C, the equivalent increase in SAT is 2.9°C. The patterns of warming are also different, the  
233 largest increases in SST typically occur in July and August, whereas the larger SAT increases are  
234 observed in November and December. The SST increase is greatest in summer due to the increase  
235 in open water, which would previously have been covered by sea ice. This heat is then released  
236 into the atmosphere during the autumn as the sea ice refreezes, producing the large SAT autumn  
237 increase. As water has a greater specific heat capacity than air, the overall SST response is smaller  
238 than the SAT response. This delayed warming effect and lower SST response have been observed  
239 and discussed in previous studies (e.g. Howell et al. (2014); Kumar et al. (2010); Screen and  
240 Simmonds (2010)).

241 The largest increases occur in the simulations with both reduced minimum albedo and increased  
242 pCO<sub>2</sub>. The mean annual increase in SST north of 60°N in these simulations is 1.3°C, with a  
243 maximum of 1.8°C in the Jul\_500\_0.2 simulation. The highest mean monthly SST increase is  
244 4.2°C in August in Jul\_500\_0.2. The mean annual SAT increase north of 60°N in the same five  
245 simulations is 4.0°C. Jul\_500\_0.2 also shows the greatest increase in mean annual SAT, with a rise  
246 of 4.8°C, whilst the 9.8°C rise in January in the Jan\_500\_0.2 simulation is the largest rise in any  
247 single month.

248 Focusing north of 80°N, the SAT changes are even greater. The Jul\_500\_0.2 mean annual  
249 increase is 8.3°C, and the increase in December of the same simulation is 19.8°C. SST increases  
250 north of 80°N, however, do not show uniformly higher increases compared to north of 60°N. The  
251 mean increase in mean annual SST across the five simulations is 1.1°C, the highest single mean  
252 annual change being 1.7°C in Jul\_500\_0.2. The greatest monthly change is higher, however, with  
253 August in Jul\_500\_0.2 showing an SST increase of 5.0°C compared to the control.

254 Figure 8 indicates that the warming north of 60°N from increased pCO<sub>2</sub> is greater than the  
255 warming seen in the reduced albedo (400 ppm) simulations (comparing the same orbit), despite  
256 there being a smaller reduction in sea ice extent. Whilst this is not also true in all cases when  
257 looking at the SST changes, the Jan\_500\_0.5, Jul\_500\_0.5 and Sep\_500\_0.5 simulations with 500  
258 ppm pCO<sub>2</sub> all have higher mean annual SSTs north of 60°N than the same orbital simulations with  
259  $\alpha_{min} = 0.2$ .

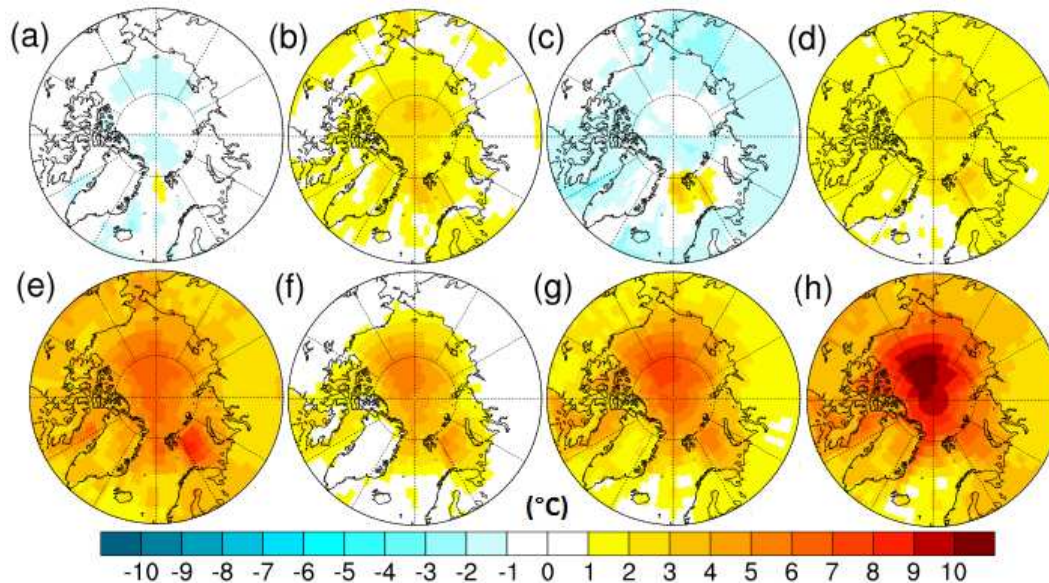


Figure 4: Mean annual SAT ( $^{\circ}\text{C}$ ) anomaly (alternative minus control) for simulations: (a) Mar\_400\_0.5 (b) Jul\_400\_0.5 (c) Jul\_300\_0.5 (d) Mod\_500\_0.5 (e) Jul\_500\_0.5 (f) Mod\_400\_0.2 (g) Mod\_500\_0.2 (h) Jul\_500\_0.2. Control simulation is Mod\_400\_0.5.

### 260 3.2.2. Energy balance

261 Using the methods of Hill et al. (2014), energy balance calculations have quantified the con-  
 262 tributions of the different components of the SAT warming (compared to the mid-Pliocene control  
 263 simulation) for the Mod\_400\_0.2 and Mod\_500\_0.5 simulations (Figure 9). These two simula-  
 264 tions are chosen to allow comparison of the differences between changing only sea ice albedo, and  
 265 changing only atmospheric  $\text{CO}_2$ . The zonal warming varies more in Mod\_400\_0.2, with very little  
 266 temperature change at latitudes south of  $60^{\circ}\text{N}$ , and more than  $4^{\circ}\text{C}$  of warming close to  $90^{\circ}\text{N}$ . The  
 267 Mod\_500\_0.5 simulation shows similar levels of warming at all latitudes north of  $60^{\circ}\text{N}$ , between  
 268  $0.5$  and  $2^{\circ}\text{C}$ .

269 North of  $60^{\circ}\text{N}$ , the largest contribution to SAT warming in Mod\_500\_0.5 is greenhouse gas  
 270 emissivity, marginally ahead of clear sky albedo. Cloud emissivity and meridional heat transport  
 271 have a small warming contribution, whilst there is a small cooling contribution due to cloud albedo.  
 272 All the individual contributions are less than  $1^{\circ}\text{C}$ . In contrast, the contribution from clear sky albedo  
 273 in the Mod\_400\_0.2 is up to  $6^{\circ}\text{C}$  at high northern latitudes. Greenhouse gas and cloud emissivity  
 274 also contribute to the warming, whilst there are cooling contributions of up to  $2^{\circ}\text{C}$  from meridional  
 275 heat transport, and  $3.5^{\circ}\text{C}$  from cloud albedo.

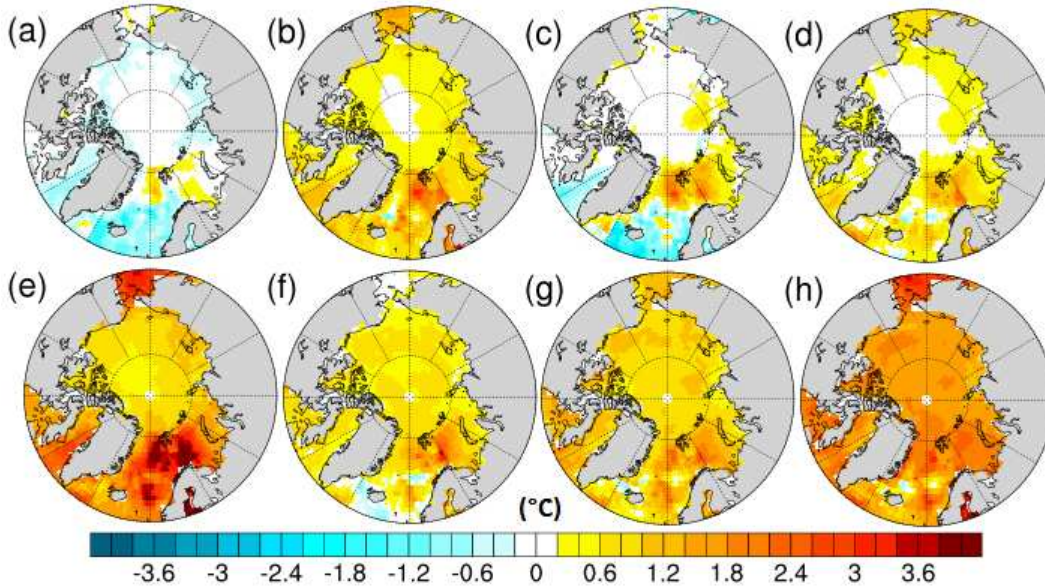


Figure 5: Mean annual SST ( $^{\circ}\text{C}$ ) anomaly (alternative minus control) for simulations: (a) Mar\_400\_0.5 (b) Jul\_400\_0.5 (c) Jul\_300\_0.5 (d) Mod\_500\_0.5 (e) Jul\_500\_0.5 (f) Mod\_400\_0.2 (g) Mod\_500\_0.2 (h) Jul\_500\_0.2. Control simulation is Mod\_400\_0.5.

### 276 3.2.3. Data-model comparison

277 Tables 2 and 3 show the data-model comparison for data sites north of  $60^{\circ}\text{N}$ . For all of the  
 278 SAT sites, and two of the SST sites, the greatest increase relative to the control simulation (denoted  
 279 as mPWP<sup>a</sup> in Tables 2 and 3) is seen in the Jul\_500\_0.2 simulation. The largest increases at the  
 280 remaining SST sites come from the Jul\_500\_0.5 simulation.

281 The discrepancy between proxy data and model mean annual SSTs has been reduced to less  
 282 than  $1^{\circ}\text{C}$  for four of the six SST estimates (ODP 907A<sup>2</sup>, ODP 910C, Colvillian and Meighen  
 283 Island). In the other two estimates, at ODP 907A<sup>1</sup> and ODP 909C, the gap between the model  
 284 temperatures and proxy estimates is greater ( $3.3^{\circ}\text{C}$  and  $6.6^{\circ}\text{C}$  respectively).

285 At each of the terrestrial data sites north of  $60^{\circ}\text{N}$ , there is an increase in mean annual SAT of at  
 286 least  $3^{\circ}\text{C}$  in comparison to the control simulation. The highest change in mean annual SAT is seen  
 287 at Beaver Pond, with an increase of  $5.1^{\circ}\text{C}$ . The model temperatures all remain cooler than the proxy  
 288 estimate, the smallest difference being  $0.4^{\circ}\text{C}$  at Lost Chicken Mine. In the control simulation,  
 289 the discrepancy was  $4.4^{\circ}\text{C}$  at this site. At only one other site, Alaska Circle, is the model-data  
 290 difference less than  $2^{\circ}\text{C}$ . At the remaining seven the difference is at least  $3^{\circ}\text{C}$ , the largest difference  
 291 being  $13.6^{\circ}\text{C}$  at Delyankir.

292 Analysis of pollen assemblages extracted from sediment at Lake El'gygytgyn ( $67.3^{\circ}\text{N}$ ,  $172.1^{\circ}\text{E}$ )  
 293 suggests that warmest monthly SATs at this location in the mid-Pliocene were approximately 16

Table 2: Summary of observational, proxy and modelled temperatures and anomalies at terrestrial data sites. All temperatures are in °C. The mPWP<sup>c</sup> simulation is Mod\_400\_0.5, mPWP<sup>a</sup> is Jul\_500\_0.2. Column (a) is the data site name and reference. Column (b) is the data site latitude (°N) and longitude (°E) co-ordinates. Column (c) is 20th century (1961 – 1990) mean annual SAT observations from Legates and Willmott (1990). Column (d) is proxy-inferred mid-Pliocene mean annual SAT. Column (e) is proxy – observation. Column (f) is simulated pre-industrial (PI) mean annual SAT. Column (g) is simulated mid-Pliocene control mean annual SAT (mPWP<sup>c</sup>). Column (h) is warmest ensemble member simulated mid-Pliocene mean annual SAT (mPWP<sup>a</sup>). Column (i) is mPWP<sup>c</sup> – PI. Column (j) is mPWP<sup>a</sup> – PI. Column (k) is mPWP<sup>c</sup> – proxy. Column (l) is mPWP<sup>a</sup> – proxy. Column (m) is percentage change (between (k) and (l)).

| (a)                      | (b)    | (c)   | (d)  | (e)  | (f)   | (g)   | (h)   | (i)  | (j)  | (k)   | (l)   | (m)  |
|--------------------------|--------|-------|------|------|-------|-------|-------|------|------|-------|-------|------|
| <b>Beaver Pond</b>       | 78.4   | -15.7 | -1.4 | 14.3 | -27.6 | -15.9 | -10.8 | 11.7 | 16.8 | -14.5 | -9.4  | 35.2 |
| Ballantyne et al. (2010) | -82.0  |       |      |      |       |       |       |      |      |       |       |      |
| Rybczynski et al. (2013) |        |       |      |      |       |       |       |      |      |       |       |      |
| <b>Lena River</b>        | 72.2   | -14.8 | 1.5  | 16.3 | -19.8 | -10.5 | -7.0  | 9.3  | 12.8 | -12.0 | -8.5  | 29.2 |
| Fradkina (1991)          | 126.0  |       |      |      |       |       |       |      |      |       |       |      |
| <b>Alaska Circle</b>     | 65.5   | -5.7  | 3.0  | 8.7  | -7.9  | -2.3  | 1.6   | 5.6  | 9.5  | -5.3  | -1.4  | 73.8 |
| Ager et al. (1994)       | -144.1 |       |      |      |       |       |       |      |      |       |       |      |
| <b>Blizkiy</b>           | 64.0   | -7.3  | 5.3  | 12.6 | -15.6 | -5.2  | -1.9  | 10.4 | 13.7 | -10.5 | -7.2  | 31.1 |
| Popova et al. (2012)     | -162.0 |       |      |      |       |       |       |      |      |       |       |      |
| <b>Nenana Valley</b>     | 64.5   | -3.7  | 3.0  | 6.7  | -7.4  | -4.0  | -0.3  | 3.4  | 7.0  | -7.0  | -3.3  | 52.5 |
| Ager et al. (1994)       | -149.1 |       |      |      |       |       |       |      |      |       |       |      |
| <b>Lost Chicken Mine</b> | 64.1   | -5.3  | 2.5  | 7.8  | -7.8  | -1.9  | 2.1   | 5.9  | 9.9  | -4.4  | -0.4  | 90.2 |
| Ager et al. (1994)       | -142.0 |       |      |      |       |       |       |      |      |       |       |      |
| <b>Bonanza Creek</b>     | 63.9   | -4.7  | 6.5  | 11.2 | -6.9  | -1.8  | 3.1   | 5.1  | 10.0 | -8.3  | -3.4  | 59.0 |
| Pound et al. (2015)      | -139.3 |       |      |      |       |       |       |      |      |       |       |      |
| <b>Delyankir</b>         | 63.0   | -10.4 | 7.4  | 17.8 | -13.1 | -9.6  | -6.2  | 3.5  | 6.9  | -17.0 | -13.6 | 19.7 |
| Popova et al. (2012)     | 133.0  |       |      |      |       |       |       |      |      |       |       |      |
| <b>Magadan District</b>  | 60.0   | -4.1  | 2.0  | 6.1  | -11.7 | -5.1  | -2.0  | 6.7  | 9.7  | -7.1  | -4.0  | 43.0 |
| Fradkina (1991)          | 150.7  |       |      |      |       |       |       |      |      |       |       |      |

Table 3: Summary of observational, proxy and modelled temperatures and anomalies at marine data sites. All temperatures are in °C. The mPWP<sup>c</sup> simulation is Mod\_400\_0.5, mPWP<sup>a</sup> is Jul\_500\_0.5 for the ODP sites, and Jul\_500\_0.2 for the other sites. Column (a) is the data site name and reference. Column (b) is the data site latitude (°N) and longitude (°E) co-ordinates. Column (c) is 20th century (1961 – 1990) mean annual SST observations from Rayner et al. (2003). Column (d) is proxy-inferred mid-Pliocene mean annual SST. Column (e) is proxy – observation. Column (f) is simulated pre-industrial (PI) mean annual SST. Column (g) is simulated mid-Pliocene control mean annual SST (mPWP<sup>c</sup>). Column (h) is warmest ensemble member simulated mid-Pliocene mean annual SST (mPWP<sup>a</sup>). Column (i) is mPWP<sup>c</sup> – PI. Column (j) is mPWP<sup>a</sup> – PI. Column (k) is mPWP<sup>c</sup> – proxy. Column (l) is mPWP<sup>a</sup> – proxy. Column (m) is percentage change (between (k) and (l)).

| (a)   | (b)            | (c)  | (d)  | (e) | (f)  | (g)  | (h) | (i)  | (j) | (k)  | (l)  | (m)  |
|---|----------------|------|------|-----|------|------|-----|------|-----|------|------|------|
| <b>ODP 907A</b> <sup>1</sup><br>Robinson (2009)       | 69.1<br>-12.4  | 2.4  | 11.7 | 9.4 | 3.8  | 5.5  | 8.2 | 1.7  | 4.2 | -6.2 | -3.5 | 43.6 |
| <b>ODP 907A</b> <sup>2</sup><br>Schreck et al. (2013) | 69.1<br>-12.4  | 2.4  | 8.5  | 6.1 | 3.8  | 5.5  | 8.2 | 1.7  | 4.2 | -3.0 | -0.3 | 90.0 |
| <b>ODP 909C</b><br>Robinson (2009)                    | 78.6<br>-3.1   | 1.1  | 10.2 | 9.1 | 1.5  | 0.4  | 3.6 | -1.1 | 2.1 | -9.8 | -6.6 | 32.7 |
| <b>ODP 910C</b><br>Knies et al. (2014)                | 80.2<br>6.4    | 0.3  | 4.1  | 3.8 | 1.9  | 0.8  | 3.3 | -1.1 | 1.4 | -3.3 | -0.8 | 75.8 |
| <b>Colvillian</b><br>Brouwers (1994)                  | 70.3<br>-150.4 | -1.5 | 1.2  | 2.7 | -1.6 | -1.0 | 0.8 | 0.6  | 2.4 | -2.4 | -0.4 | 83.3 |
| <b>Meighen Island</b><br>Fyles et al. (1991)          | 79.0<br>-99.0  | -1.8 | 1.7  | 3.5 | -1.4 | -0.1 | 1.3 | 1.3  | 2.7 | -1.8 | -0.4 | 77.8 |

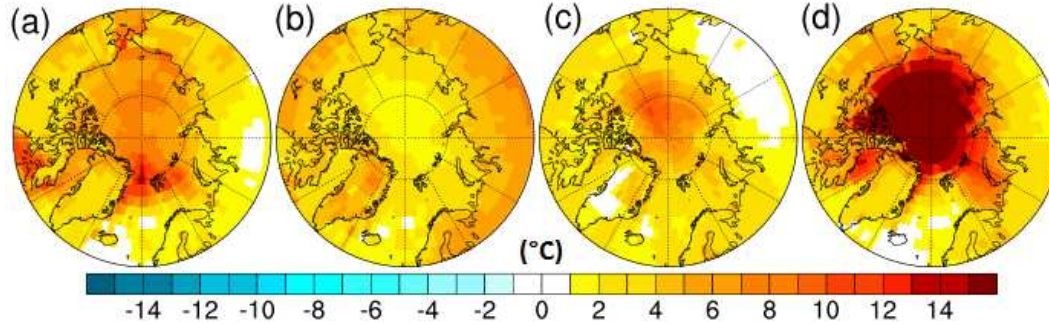


Figure 6: Seasonal SAT ( $^{\circ}\text{C}$ ) anomalies (compared to control) for the Jul\_500\_0.2 simulation for (a) FMA (b) MJJ (c) ASO (d) NDJ. Control simulation is Mod\_400\_0.5.

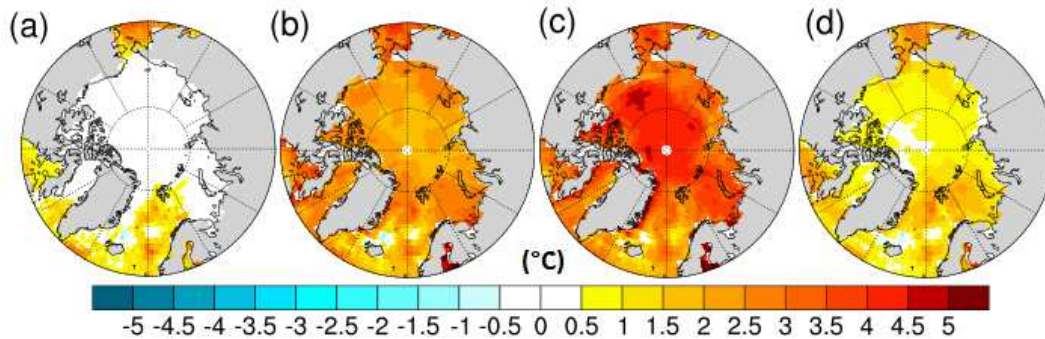


Figure 7: Seasonal SST ( $^{\circ}\text{C}$ ) anomalies (compared to control) for the Jul\_500\_0.2 simulation for (a) FMA (b) MJJ (c) ASO (d) NDJ. Control simulation is Mod\_400\_0.5.

294 –  $17^{\circ}\text{C}$  (Brigham-Grette et al., 2013; Andreev et al., 2014). The warmest monthly temperature in  
 295 the control simulation shows a temperature of  $14.4^{\circ}\text{C}$  at the location of Lake El'gygytyn,  $1.6 -$   
 296  $2.6^{\circ}\text{C}$  cooler than the indications from proxy data. The model fails to achieve the level of warming  
 297 indicated by the data, as with the mean annual SATs shown in Table 2, but with a smaller tempera-  
 298 ture discrepancy. Out of the rest of the ensemble, four simulations (Jan\_400\_0.2, Jul\_400\_0.2,  
 299 Jul\_300\_0.5 and Jul\_300\_0.2) produced maximum monthly SAT values within the  $16 - 17^{\circ}\text{C}$   
 300 range, with a further four (Jul\_400\_0.5, Jan\_500\_0.5, Jul\_500\_0.5 and Jul\_500\_0.2) exceeding  
 301 this range for warmest monthly mean. As only mean warmest month temperatures were available,  
 302 Lake El'gygytyn temperatures do not feature in Tables 2 and 4.

303 Tables 2 and 3 also show the mid-Pliocene warming at each site for data and models, using  
 304 differences between the proxy data temperatures and 20th century observations of SAT (Legates  
 305 and Willmott, 1990) and SST (Rayner et al., 2003), and the differences between the simulated mid-  
 306 Pliocene and pre-industrial temperatures (columns (e) and (i) respectively). The model warming

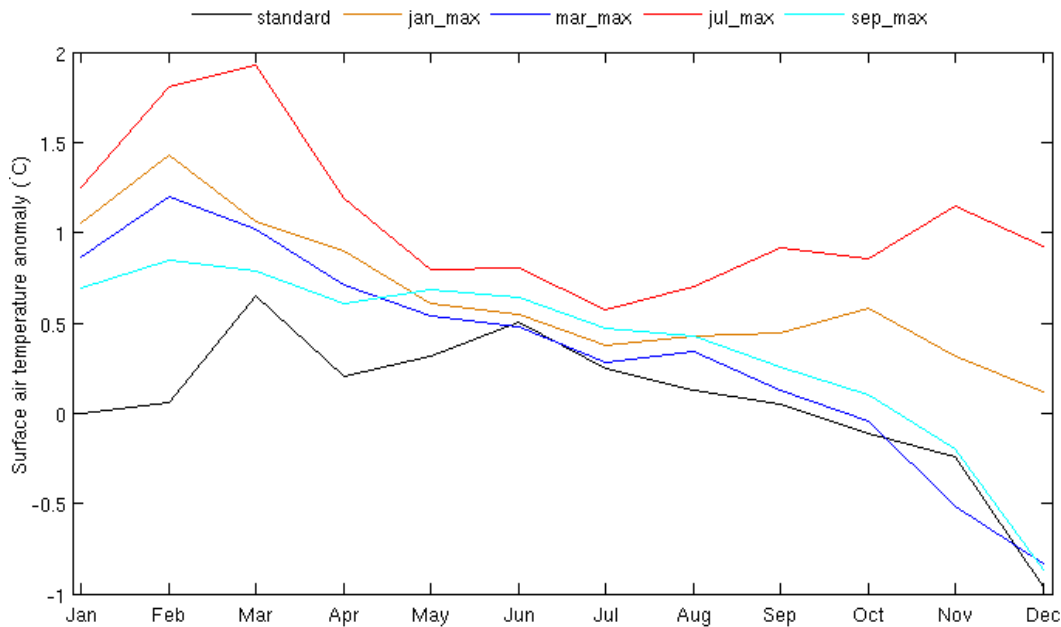


Figure 8: Mean annual cycle of the difference in mean SAT north of 60°N between the 5 simulations with 500 ppm pCO<sub>2</sub> and  $\alpha_{min} = 0.5$ , and the 5 with 400 ppm pCO<sub>2</sub> and  $\alpha_{min} = 0.2$ . Difference shown is 500\_0.5 minus 400\_0.2, for the same orbital configurations.

307 exceeds the data warming only at the Magadan District terrestrial site (by 0.6°C). The greatest SAT  
 308 difference is at Delyankir (14.3°C), whilst the largest SST difference is at ODP 909C (10.2°C).  
 309 At ODP sites 909C and 910C, the pre-industrial SSTs are actually warmer than those from the  
 310 mid-Pliocene simulation (1.5°C and 1.9°C compared to 0.4°C and 0.8°C respectively, see Table 3).  
 311 An important caveat to note is that the observations are from the 20th century, so are likely to be  
 312 warmer than temperatures from the pre-industrial, for which the model simulation comparisons are  
 313 run.

314 At six of the terrestrial sites, the SAT increase compared to the control in the warmest en-  
 315 semble member (Jul\_500\_0.2) is greater than the difference between the data and model warming  
 316 at each site. Consequently, the temperature difference between the pre-industrial simulation and  
 317 Jul\_500\_0.2 exceeds the difference between the modern observations and the proxy estimates at  
 318 each site. This shows a degree of agreement between the proxies and the simulation.

319 Table 4 shows the greatest increase in December SAT (consistently largest SAT increase of all  
 320 months) in the ensemble from the control, at each terrestrial data site. Out of the nine data sites,  
 321 the largest monthly change at six of them is smaller than the difference between the mean annual  
 322 temperature estimates from the proxy data and control simulation. Table 5 shows the greatest  
 323 increase in August SST (consistently largest SST increase of all months) in the ensemble for each

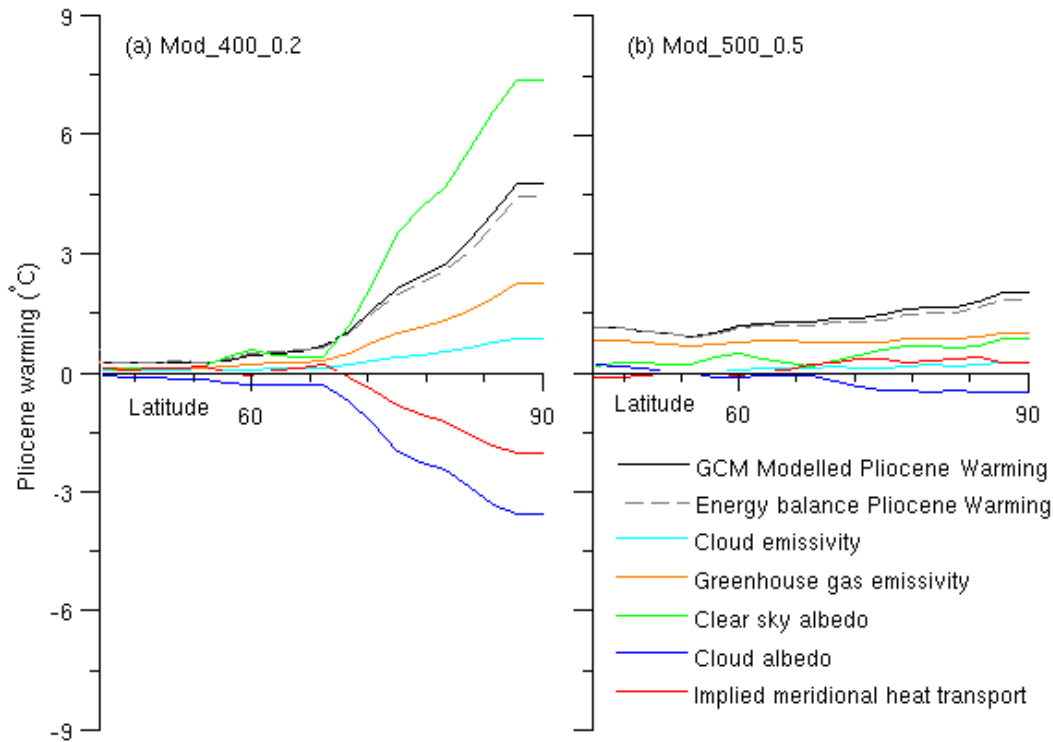


Figure 9: Energy balance analysis north of 30°N for (a) Mod\_400\_0.2 (b) Mod\_500\_0.2. Plots show zonal mean warming for each of the energy balance components, along with the zonal mean SAT increase compared to the mid-Pliocene control, and the approximated zonal mean SAT increase from the energy balance contributions.

324 data site. At four sites (ODP 907A<sup>2</sup>, ODP 910C, Colvillian and Meighen Island), the maximum  
 325 monthly increase exceeds the model-data mean annual anomaly for the control. Only for ODP  
 326 907A<sup>1</sup> and ODP 909C would the maximum monthly increase not be enough to close the data-  
 327 model disparity if it was sustained year-round.

## 328 4. Discussion

### 329 4.1. Sea ice

330 Figure 2(c) indicates that a change in orbital forcing is sufficient to cause the mid-Pliocene  
 331 Arctic to become ice-free at some point during the summer in HadCM3. In the Jul\_400\_0.5 simu-  
 332 lation, sea ice extent dropped to  $0.37 \times 10^6 \text{ km}^2$  in September. However, when the atmospheric CO<sub>2</sub>  
 333 concentration was also lowered to 300 ppm, no simulation was ice-free at any point. This implies  
 334 that knowing the atmospheric CO<sub>2</sub> concentration to within 100 ppm is important to ascertaining  
 335 whether the mid-Pliocene Arctic saw sea ice-free conditions (using HadCM3).

Table 4: Simulated December (month with largest monthly increase between warmest ensemble member and control) SATs for mid-Pliocene control simulation (mPWP<sup>c</sup>, Mod\_400\_0.5), and warmest ensemble member (mPWP<sup>a</sup>, Jul\_500\_0.2) at terrestrial sites in Table 2. All temperatures in °C. Column (a) is site name. Column (b) is mPWP<sup>c</sup> – proxy mean annual temperature anomaly ((k) in Table 2)). Column (c) is simulated December SAT in mPWP<sup>c</sup>. Column (d) is simulated December SAT in mPWP<sup>a</sup>. Column (e) is December mPWP<sup>a</sup> – December mPWP<sup>c</sup>.

| (a)                      | (b)   | (c)   | (d)   | (e) |
|--------------------------|-------|-------|-------|-----|
| <b>Beaver Pond</b>       | -14.5 | -31.2 | -24.2 | 7.0 |
| <b>Lena River</b>        | -12.0 | -31.6 | -25.4 | 6.2 |
| <b>Alaska Circle</b>     | -5.3  | -18.7 | -12.1 | 6.6 |
| <b>Blizkiy</b>           | -10.5 | -21.9 | -17.1 | 4.8 |
| <b>Nenana Valley</b>     | -7.0  | -21.4 | -14.2 | 7.2 |
| <b>Lost Chicken Mine</b> | -4.4  | -17.4 | -11.1 | 6.3 |
| <b>Bonanza Creek</b>     | -8.3  | -18.6 | -12.0 | 6.6 |
| <b>Delyankir</b>         | -17.0 | -33.2 | -31.3 | 1.9 |
| <b>Magadan District</b>  | -7.1  | -25.5 | -22.5 | 3.0 |

Table 5: Simulated August (month with largest monthly increase between warmest ensemble member and control) SSTs for mid-Pliocene control simulation (mPWP<sup>c</sup>, Mod\_400\_0.5), and warmest ensemble member (mPWP<sup>a</sup>, Jul\_500\_0.5 for ODP 907A and ODP 909C, Jul\_500\_0.2 for the other sites) at sites from Table 3. All temperatures in °C. Column (a) is site name. Column (b) is mPWP<sup>c</sup> – proxy mean annual temperature anomaly ((k) in Table 3). Column (c) is August SST in mPWP<sup>c</sup>. Column (d) is August SST in mPWP<sup>a</sup>. Column (e) is August mPWP<sup>a</sup> – August mPWP<sup>c</sup>.

| (a)                         | (b)  | (c) | (d)  | (e) |
|-----------------------------|------|-----|------|-----|
| <b>ODP 907A<sup>1</sup></b> | -6.2 | 7.7 | 11.7 | 4.0 |
| <b>ODP 907A<sup>2</sup></b> | -3.0 | 7.7 | 11.7 | 4.0 |
| <b>ODP 909C</b>             | -9.8 | 3.2 | 7.0  | 3.8 |
| <b>ODP 910C</b>             | -3.3 | 3.1 | 6.5  | 3.4 |
| <b>Colvillian</b>           | -2.4 | 0.5 | 5.9  | 5.4 |
| <b>Meighen Island</b>       | -1.8 | 3.7 | 7.4  | 3.7 |

336 The Jan\_500\_0.5 simulation achieves ice-free conditions in addition to Jul\_500\_0.5. Other  
337 orbital simulations, notably the standard orbital configuration, do not. This is an important result  
338 as it appears to suggest that the Arctic sea ice in the mid-Pliocene is more sensitive to changes that  
339 result due to the different orbital configurations than an increase in 100 ppm pCO<sub>2</sub>.

340 The difference between some simulations producing ice-free conditions under 400 ppm but not  
341 under 300 ppm is also an important result, as atmospheric CO<sub>2</sub> during the mPWP is likely to have  
342 varied during the period. Based on the results of these simulations, the coinciding of particular  
343 orbital configurations with variations in pCO<sub>2</sub> is crucial to whether the Arctic becomes ice-free or  
344 not in HadCM3. This suggests that much tighter age control on proxy data will be required in order  
345 to make a consistent data-model comparison.

346 Sea ice-free conditions in the mid-Pliocene Arctic would contradict Darby (2008), who show  
347 evidence from iron grains in the ACEX core (located at 87.5°N, -138.3°E) implying that perennial  
348 sea ice was present in the Arctic at least as far back as 14 Myr ago. The samples from the core  
349 represent approximately 1 ka, sampled at an average rate through the core of 0.17 Ma ( $\pm$  0.35). It  
350 is possible that there were sea ice-free events during the mid-Pliocene which were missed by the  
351 sampling, although Darby (2008) asserts that the probability of each of the 155 ACEX samples  
352 missing a time where seasonal ice was present is low. The presence of the sea ice proxy IP<sub>25</sub> (Belt  
353 et al., 2007; Brown et al., 2014) in mid-Pliocene sediment from ODP 910C shown in Knies et al.  
354 (2014), indicates perennial sea ice conditions at 80°N in the Atlantic sector of the mid-Pliocene  
355 Arctic Ocean.

356 When minimum albedo is reduced to 0.2, the orbital configuration is less significant, as the  
357 sea ice disappears completely in each simulation from August to October. This implies that if this  
358 is an appropriate parameterisation within HadCM3 for the mPWP, the orbital configuration is less  
359 relevant in relation to the issue of the Arctic being ice-free, although it still makes a difference to  
360 the timing and duration of the ice-free conditions. The Jan\_400\_0.2 and Jul\_400\_0.2 simulations  
361 have faster declines from June to July, and slower recoveries after October, which is likely to have  
362 an effect on the surface temperatures. Even under 300 ppm pCO<sub>2</sub>, all simulations produce ice-  
363 free conditions, with the main effect of the lower pCO<sub>2</sub> appearing to be facilitating a faster sea ice  
364 recovery in the winter. Increasing to 500 ppm pCO<sub>2</sub> extends the period time over which the ice-free  
365 summer conditions exist, and slows down the winter recovery.

366 An important caveat in any assessment of the sensitivity of simulated Arctic sea ice is that  
367 conclusions are based on the assumption that HadCM3 is able to simulate mid-Pliocene sea ice  
368 well. Howell et al. (2015) suggested that, based on the limited proxy data evidence regarding  
369 Pliocene Arctic sea ice, that HadCM3 had the closest agreement with the conclusions of the data in  
370 its mPWP simulation of all the PlioMIP models, although other models' CMIP5 sea ice simulations  
371 matched modern observations more closely (Shu et al., 2015).

372 Within the PlioMIP ensemble, HadCM3 was not one of the four models which simulated an  
373 ice-free Arctic summer, but did have the lowest summer extent of the four simulations which main-  
374 tained ice year-round (Howell et al., 2015). In light of the sensitivity which HadCM3 displays  
375 with regard to orbit, atmospheric CO<sub>2</sub> and albedo parameterisation, similar assessments of other  
376 models, both with summer sea ice and without, would provide interesting insights.

377 4.2. Temperatures

378 Using CAM3, an atmosphere-only model, Ballantyne et al. (2013) ran a simulation of the  
379 mPWP where Arctic sea ice is absent year round, and showed warming of 10°C to 15°C extending  
380 into the continental interior. Subsequently a much closer, although not complete, agreement with  
381 proxy data SAT estimates than the control simulation was achieved. However, as stated in Ballan-  
382 tyne et al. (2013), a complete absence of sea ice is not likely to be a realistic mid-Pliocene boundary  
383 condition. The ensemble simulations with the highest sea ice reduction (Figure 2(b)) produce sea  
384 ice-free conditions for almost half the year, but by March the extent has recovered to 82.4% of the  
385 control value, albeit with a 38.2% drop in mean thickness.

386 A fully coupled GCM can not maintain the latent heat transfer from ocean to atmosphere  
387 throughout the year that is seen in the atmosphere only simulation of Ballantyne et al. (2013),  
388 which appears to be required to provide a consistent level of temperature increase in order to close  
389 the data-model mismatch. Even if the temperature increases at each site in December were repli-  
390 cated in all other months, this would not be sufficient to produce agreement between models and  
391 proxy data temperatures at more than half the terrestrial sites (Table 4).

392 At the marine sites, the data-model SST difference is less than 1°C for all but ODP 907A<sup>1</sup> and  
393 ODP 909C. In the warmest simulation at these two sites (Jul\_500\_0.5), the data-model difference  
394 is 3.5°C and 6.6°C respectively. If the maximum monthly SST increase compared to the control  
395 (August) were maintained year-round, the data-model difference would reduce to 2.2°C and 6.0°C  
396 respectively. Differences between models and the SST estimates for these sites from Robinson  
397 (2009) remain, in contrast to the closer agreement with the more recent SST estimates in Schreck  
398 et al. (2013) and Knies et al. (2014) at similar locations.

399 The discrepancy is lower when comparing the temperature increases for models and data, as  
400 opposed to just the temperatures, and at some sites the model warming in some ensemble members  
401 is close to or exceeds the data warming. However, at three terrestrial and four marine sites, the  
402 model warming is still lower than the data warming, even in the warmest simulations.

403 A caveat that must be considered when comparing the model and proxy temperatures is that as  
404 the proxy data covers 3.3 to 3.0 Myr ago (with wider temporal ranges in the terrestrial data), the  
405 samples used may not all be exactly the same age. Expecting the models to achieve the desired level  
406 of warming at all sites under the same combination of boundary conditions may not be realistic.  
407 The influence that the orbit has on simulated temperatures also questions the value of a comparison  
408 of a simulation with a proxy estimate representing the average of several different orbital forcings.

409 The simulations with atmospheric CO<sub>2</sub> increased to 500 ppm have higher SATs than the sim-  
410 ulations with  $\alpha_{min}$  reduced to 0.2 in most months, but larger sea ice extents (Figures 2, 8). The  
411 breakdown of the different contributions to high latitude warming is shown in Figure 9. Clear sky  
412 albedo is the dominant contributor in the  $\alpha_{min} = 0.2$  simulations, coming as a result of the change  
413 to the albedo parameterisation and subsequent exposure of greater areas of open water as more ice  
414 melts, which will then lead to temperature increases.

415 Greenhouse gas emissivity is, marginally ahead of clear sky albedo, the largest contributor to  
416 warming in the 500 ppm simulations. In these runs, the higher atmospheric CO<sub>2</sub> concentrations  
417 lead to higher temperatures, which leads to melting sea ice. Feedbacks will enhance both sea

418 ice melt and warming in both sets of simulations. However, in the  $\alpha_{min} = 0.2$  runs, it is initial  
419 reductions in sea ice which then drive temperature increases, whilst the reverse is the case in the  
420 500 ppm pCO<sub>2</sub> simulations.

421 In the Mod\_400\_0.2 simulation, cloud albedo contributed up to 4°C of cooling at high lat-  
422 itudes compared to the control simulation (Figure 9). The Mod\_500\_0.5 simulation showed a  
423 much lower cooling contribution due to cloud albedo effects at high latitudes in Mod\_400\_0.2,  
424 and other simulations with reduced minimum albedo. The overall surface albedo north of 60°N is  
425 lower in Mod\_400\_0.2 compared to Mod\_500\_0.5, due to the reduced sea ice in Mod\_400\_0.2.  
426 Consequently, the presence of clouds at high latitudes increases the planetary albedo more in  
427 Mod\_400\_0.2 than in Mod\_500\_0.5. The difference in the cloud albedo contributions in the energy  
428 balance analysis reflect this.

429 As the results shown in Figure 8 indicate, changes to the model that directly reduce sea ice,  
430 such as the changes made to sea ice albedo, do result in greater high latitude temperatures, but do  
431 not appear to be as effective as changes which have a more direct impact on temperature changes,  
432 such as atmospheric CO<sub>2</sub> increases. This suggests it may be difficult to achieve the large tem-  
433 perature increases necessary to significantly reduce the data-model disagreements through model  
434 adjustments which only indirectly lead to higher temperatures. Alternatively, if models cannot sim-  
435 ulate sufficiently warm mean annual temperatures at the proxy data locations, even with significant  
436 forcings at high latitudes, then the possibility that the temperatures inferred from proxy data relate  
437 to maximum or growing season temperatures, as opposed to mean annual seems more likely.

## 438 5. Conclusions

439 The results in this paper emphasise the uncertainty with regards to the state of sea ice in the  
440 mid-Pliocene Arctic. Howell et al. (2015) demonstrated the range of summer sea ice extents from  
441 various models, whilst these results show that forcing uncertainties are sufficient, in the simulation  
442 of HadCM3, to make a difference between seasonal and perennial sea ice coverage. Results seen in  
443 this paper and Howell et al. (2015) give a wide range of potential states of mid-Pliocene Arctic sea  
444 ice cover derived from multiple climate models. This demonstrates the need for greater coverage  
445 of sea ice proxy data for the mid-Pliocene, which can help to identify the most suitable model and  
446 forcing combination which reflects the state of sea ice best. Orbital sensitivity to sea ice cover  
447 suggests that it may be difficult. If the sea ice cover in the mid-Pliocene moved between seasonal  
448 and perennial coverage depending on the orbital configuration, then the proxy information would  
449 have to be highly constrained in time to identify these changes.

450 Given the effect on the SATs and SSTs which are associated with the variations in sea ice  
451 cover, the ability to more accurately constrain the sea ice conditions in the mid-Pliocene may also  
452 help constrain the resulting high latitude temperature changes. However, it is likely to be difficult  
453 to distinguish between the various ice-free scenarios which are seen in the ensemble. Proxy data  
454 would need to indicate the timing of the disappearance and freeze-up of the sea ice, or give an  
455 indication to other metrics, such as winter thickness, for which no proxy indicator currently exists.

456 At the terrestrial sites, with the exception of Lost Chicken Mine and Alaska Circle, no simula-  
457 tion was able to reduce the data-model discrepancies for mean annual temperature estimates to less  
458 than 3°C, with some discrepancies still exceeding 8°C. Modelled and proxy SSTs showed closer  
459 agreement, with model temperatures less than 1°C lower than four of the six proxy SSTs in Table 3.  
460 Uncertainties associated with the temperature reconstructions are specified for some terrestrial data  
461 sites (Salzmann et al., 2013; Pound et al., 2015). With the exception of Bonanza Creek, none of the  
462 alternative anomalies in Table 2 are less than any of the given uncertainties. Errors associated with  
463 the SST reconstruction methods are less than 2°C (Dowsett et al., 2009), so four of the alternative  
464 anomalies in Table 3 are within the uncertainties. The effect of even a very dramatic reduction in  
465 the total sea ice cover is not capable of producing agreement at many sites.

466 As suggested in Ballantyne et al. (2013), a year-round absence of sea ice is perhaps the only way  
467 that such high temperature increases can be maintained throughout the year in order to get close  
468 agreement between models and data. However, there is evidence for the presence of mid-Pliocene  
469 Arctic sea ice (e.g. Darby (2008); Polyak et al. (2010); Knies et al. (2014)), and maintaining ice-  
470 free conditions in a coupled AOGCM would require a source of heat into the Arctic during the  
471 winter months to prevent freeze-up until the spring. A severely depleted, but not absent, winter sea  
472 ice cover might allow for sufficient temperature increase to reduce the data-model mismatch. It is  
473 clear from the results of this study that if there is to be closer agreement between proxy and model  
474 temperatures, then even the dramatic reductions in sea ice seen in this study will not be sufficient,  
475 although they can play an important role in reducing the differences between proxy data and model  
476 results. Increased spatial coverage and understanding of the proxy data is crucial to ensure optimal  
477 comparison of model and proxy temperatures in the mid-Pliocene.

## 478 **Acknowledgements**

479 F.W. Howell acknowledges NERC for the provision of a doctoral training grant. F.W. Howell  
480 and A.M. Haywood acknowledge that the research leading to these results has received funding  
481 from the European Research Council under the European Union's Seventh Framework Programme  
482 (FP7/2007-2013)/ERC grant agreement no. 278636. A.M. Dolan is acknowledged for providing  
483 access to the orbital forcing calculations and files. D.J. Hill is acknowledged for providing the code  
484 for the energy balance calculations.

## **References**

- Ager, T. A., Matthews, J. V., Yeend, W., 1994. Pliocene terrace gravels of the ancestral Yukon River near Circle, Alaska: Palynology, paleobotany, paleoenvironmental reconstruction and regional correlation. *Quaternary International* 22, 185–206.
- Andreev, A. A., Tarasov, P. E., Wennrich, V., Raschke, E., Herzsuh, U., Nowaczyk, N. R., Brigham-Grette, J., Melles, M., 2014. Late Pliocene and early Pleistocene vegetation history of northeastern Russian Arctic inferred from the Lake El'gygytyn pollen record. *Climate of the Past* 10 (3), 1017–1039.

- Badger, M., Schmidt, D., Mackensen, A., Pancost, R., 2013. High-resolution alkenone palaeobarometry indicates relatively stable pCO<sub>2</sub> during the Pliocene (3.3-2.8 Ma). *Philos. Trans. R. Soc. A* 68, 20130094.
- Ballantyne, A., Greenwood, D., Damste, J., Csank, A., Eberle, J., Rybczynski, N., 2010. Significantly warmer Arctic surface temperatures during the Pliocene indicated by multiple independent proxies. *Geology* 38 (7), 603–606.
- Ballantyne, A., Axford, Y., Miller, G., Otto-Bliesner, B., Rosenbloom, N., White, J., 2013. The amplification of Arctic terrestrial surface temperatures by reduced sea-ice extent during the Pliocene. *Palaeogeography Palaeoclimatology Palaeoecology* 386, 59–67.
- Belt, S., Masse, G., Rowland, S., Poulin, M., Michel, C., LeBlanc, B., 2007. A novel chemical fossil of palaeo sea ice: IP<sub>25</sub>. *Organic Geochemistry* 38 (1), 16–27.
- Brigham-Grette, J., Melles, M., Minyuk, P., Andreev, A., Tarasov, P., DeConto, R., Koenig, S., Nowaczyk, N., Wennrich, V., Rosén, P., Haltia, E., Cook, T., Gebhardt, C., Meyer-Jacob, C., Snyder, J., Herzschuh, U., 2013. Pliocene warmth, polar amplification, and stepped Pleistocene cooling recorded in NE Arctic Russia. *Science* 340 (6139), 1421–1427.
- Brouwers, E. M., 1994. Late Pliocene paleoecologic reconstructions based on ostracode assemblages from the Sagavanirktok and Gubik formations, Alaskan North Slope. *Arctic*, 16–33.
- Brown, T., Belt, S., Tatarek, A., Mundy, C., 2014. Source identification of the Arctic sea ice proxy IP<sub>25</sub>. *Nature Communications* 5 (3).
- Bryan, K., 1969. Climate and the ocean circulation III The ocean model. *Mon Weather Rev* 97, 806–827.
- Cattle, H., Crossley, J., 1995. Modeling Arctic climate change. *Philosophical Transactions of the Royal Society A-Mathematical, Physical and Engineering Sciences* 352 (1699), 201–213.
- Cox, P., Betts, R., Bunton, C., Essery, R., Rowntree, P., Smith, J., 1999. The impact of new land surface physics on the GCM simulation of climate and climate sensitivity. *Climate Dynamics* 15 (3), 183–203.
- Cronin, T. M., Whatley, R., Wood, A., Tsukagoshi, A., Ikeya, N., Brouwers, E. M., Briggs, W. M., 1993. Microfaunal evidence for elevated Pliocene temperatures in the Arctic ocean. *Paleoceanography* 8 (2), 161–173.
- Curry, J. A., Schramm, J. L., Ebert, E. E., 1995. Sea ice-albedo climate feedback mechanism. *Journal of Climate* 8 (2), 240–247.
- Darby, D. A., 2008. Arctic perennial ice cover over the last 14 million years. *Paleoceanography* 23, PA1S07.

- Dowsett, H., Foley, K., Stoll, D., Chandler, M., Sohl, L., Bentsen, M., Otto-Bliesner, B., Bragg, F., Chan, W.-L., Contoux, C., Dolan, A., Haywood, A., Jonas, J., Jost, A., Kamae, Y., Lohmann, G., Lunt, D., Nisancioglu, K., Abe-Ouchi, A., Ramstein, G., Riesselman, C., Robinson, M., Salzmann, U., Stepanek, C., Strother, S., Ueda, H., Yan, Q., Zhang, Z., 2013. Sea Surface Temperature of the mid-Piacenzian Ocean: A Data-Model Comparison. *Sci. Rep.* 3, 149–163.
- Dowsett, H., Haywood, A., Valdes, P., Robinson, M., Lunt, D., Hill, D., Stoll, D., Foley, K., 2011. Sea surface temperatures of the mid-Piacenzian Warm Period: A comparison of PRISM3 and HadCM3. *Palaeogeography Palaeoclimatology Palaeoecology* 309 (1-2), 83–91.
- Dowsett, H., Robinson, M., Foley, K., 2009. Pliocene three-dimensional global ocean temperature reconstruction. *Climate of the Past* 5 (4), 769–783.
- Dowsett, H. J., Robinson, M. M., Haywood, A. M., Salzmann, U., Hill, D. J., Sohl, L., Chandler, M. A., Williams, M., Foley, K., Stoll, D., 2010. The PRISM3D paleoenvironmental reconstruction. *Stratigraphy* 7 (2-3), 123–139.
- Edwards, J., Slingo, A., 1996. Studies with a flexible new radiation code. 1: Choosing a configuration for a large-scale model. *Quarterly Journal of the Royal Meteorological Society* 122 (531), 689–719.
- Fradkina, A. F., 1991. Abstracts of the Joint US/USSR Workshop on Pliocene Palaeoclimates eds. Thompson, R.S., Borisoca, O.K. and Svetlitskaya, T.V., pp22.
- Fyles, J., Marincovich Jr, L., Matthews Jr, J., Barendregt, R., 1991. Unique mollusc find in the Beaufort Formation (Pliocene) on Meighen Island, Arctic Canada. *Current Research, Part B, Geological Survey of Canada, Paper 91*, 105–112.
- Gordon, C., Cooper, C., Senior, C. A., Banks, H., Gregory, J. M., Johns, T. C., Mitchell, J. F. B., Wood, R. A., 2000. The simulation of SST, sea ice extents and ocean heat transports in a version of the Hadley Centre coupled model without flux adjustments. *Climate Dynamics* 16 (2-3), 147–168.
- Gregory, D., Shutts, G., Mitchell, J., 1998. A new gravity-wave-drag scheme incorporating anisotropic orography and low-level wave breaking: Impact upon the climate of the UK Meteorological Office Unified Model. *Quarterly Journal of the Royal Meteorological Society* 124 (546), 463–493.
- Haywood, A., Valdes, P., 2004. Modelling Pliocene warmth: contribution of atmosphere, oceans and cryosphere. *Earth and Planetary Science Letters* 218 (3-4), 363–377.
- Haywood, A. M., Dowsett, H. J., Robinson, M. M., Stoll, D. K., Dolan, A. M., Lunt, D. J., Otto-Bliesner, B. L., Chandler, M. A., 2011. Pliocene Model Intercomparison Project (PlioMIP): experimental design and boundary conditions (Experiment 2). *Geosci. Model Dev.* 4 (3), 571–577.

- Haywood, A. M., Hill, D. J., Dolan, A. M., Otto-Bliesner, B. L., Bragg, F. J., Chan, W. L., Chandler, M. A., Contoux, C., Dowsett, H. J., Jost, A., Kamae, Y., Lohmann, G., Lunt, D. J., Abe-Ouchi, A., Pickering, S. J., Ramstein, G., Rosenbloom, N. A., Salzmann, U., Sohl, L., Stepanek, C., Ueda, H., Yan, Q., Zhang, S. Z., 2013. Large-scale features of Pliocene climate: results from the Pliocene Model Intercomparison Project. *Clim. Past* 9 (1), 191–209.
- Hibler, W. D., 1979. A dynamic-thermodynamic sea ice model. *Journal of Physical Oceanography* 9, 815–846.
- Hill, D. J., Haywood, A. M., Lunt, D. J., Hunter, S. J., Bragg, F. J., Contoux, C., Stepanek, C., Sohl, L., Rosenbloom, N. A., Chan, W. L., Kamae, Y., Zhang, Z., Abe-Ouchi, A., Chandler, M. A., Jost, A., Lohmann, G., Otto-Bliesner, B. L., Ramstein, G., Ueda, H., 2014. Evaluating the dominant components of warming in Pliocene climate simulations. *Climate of the Past* 10 (1), 79–90.
- Howell, F. W., Haywood, A. M., Dolan, A. M., Dowsett, H. J., Francis, J. E., Hill, D. J., Pickering, S. J., Pope, J. O., Salzmann, U., Wade, B. S., 2014. Can uncertainties in sea ice albedo reconcile patterns of data-model discord for the Pliocene and 20th/21st centuries? *Geophysical Research Letters* 41 (6), 2011–2018.
- Howell, F. W., Haywood, A. M., Otto-Bliesner, B. L., Bragg, F., Chan, W.-L., Chandler, M. A., Contoux, C., Kamae, Y., Abe-Ouchi, A., Rosenbloom, N. A., Stepanek, C., Zhang, Z., 2015. Arctic sea ice in the PlioMIP ensemble: is model performance for modern climates a reliable guide to performance for the past or the future? *Climate of the Past Discussions* 11 (2), 1263–1312.
- Kellogg, W., 1975. Climatic feedback mechanisms involving the polar regions. *Climate of the Arctic*, 111–116.
- Knies, J., Cabedo-Sanz, P., Belt, S. T., Baranwal, S., Fietz, S., Rosell-Melé, A., 2014. The emergence of modern sea ice cover in the Arctic Ocean. *Nat. Commun.* 5:5608.
- Kumar, A., Perlwitz, J., Eischeid, J., Quan, X., Xu, T., Zhang, T., Hoerling, M., Jha, B., Wang, W., 2010. Contribution of sea ice loss to Arctic amplification. *Geophysical Research Letters* 37.
- Laskar, J., Robutel, P., Joutel, F., Gastineau, M., Correia, A., Levrard, B., 2004. A long-term numerical solution for the insolation quantities of the Earth. *Astronomy and Astrophysics* 428, 261–285.
- Legates, D., Willmott, C., 1990. Mean seasonal and spatial variability in global surface air temperature. *Theor. Appl. Climatol.* 41, 11–21.
- Mattingsdal, R., Knies, J., Andreassen, K., Fabian, K., Husum, K., Grøsfjeld, K., Schepper, S. D., 2014. A new 6 Myr stratigraphic framework for the Atlantic–Arctic gateway. *Quaternary Science Reviews* 92, 170 – 178, {APEX} II: Arctic Palaeoclimate and its Extremes.

- Maykut, G., 1978. Energy exchange over young sea ice in the central Arctic. *Journal Of Geophysical Research - Oceans* 83 (C7), 3646–3658.
- Maykut, G., Untersteiner, N., 1971. Some results from a time-dependent thermodynamic model of sea ice. *Journal of Geophysical Research* 76 (6), 1550–1575.
- Moran, K., Backman, J., Brinkhuis, H., Clemens, S. C., Cronin, T., Dickens, G. R., Eynaud, F., Gattacceca, J., Jakobsson, M., Jordan, R. W., Kaminski, M., King, J., Koc, N., Krylov, A., Martinez, N., Matthiessen, J., McInroy, D., Moore, T. C., Onodera, J., O'Regan, M., Pälike, H., Rea, B., Rio, D., Sakamoto, T., Smith, D. C., Stein, R., St John, K., Suto, I., Suzuki, N., Takahashi, K., Watanabe, M., Yamamoto, M., Farrel, J., Frank, M., Kubik, P., Jokat, W., Kristoffersen, Y., 2006. The Cenozoic palaeoenvironment of the Arctic Ocean. *Nature* 441 (7093), 601–605.
- Nelson, R. E., Carter, L., 1985. Pollen analysis of a Late Pliocene and Early Pleistocene section from the Gubik Formation of Arctic Alaska. *Quaternary Research* 24 (3), 295 – 306.
- Pagani, M., Liu, Z., LaRiviere, J., Ravelo, A. C., 2010. High Earth-system climate sensitivity determined from Pliocene carbon dioxide concentrations. *Nature Geoscience* 3 (1), 27–30.
- Perovich, D., Polashenski, C., 2012. Albedo evolution of seasonal Arctic sea ice. *Geophysical Research Letters* 39.
- Polyak, L., Alley, R. B., Andrews, J. T., Brigham-Grette, J., Cronin, T. M., Darby, D. A., Dyke, A. S., Fitzpatrick, J. J., Funder, S., Holland, M. M., Jennings, A. E., Miller, G. H., O'Regan, M., Savelle, J., Serreze, M., St John, K., White, J. W. C., Wolff, E., 2010. History of sea ice in the Arctic. *Quaternary Science Reviews* 29 (15-16), 1757–1778.
- Popova, S., Utescher, T., Gromyko, D., 2012. Palaeoclimate evolution in siberia and the russian far east from the oligocene to pliocene: Evidence from fruit and seed floras.
- Pound, M. J., Lowther, R. I., Peakall, J., Chapman, R. J., Salzmann, U., 2015. Palynological evidence for a warmer boreal climate in the Late Pliocene of the Yukon Territory, Canada. *Palynology* 39 (1), 91–102.
- Rayner, N. A., Parker, D. E., Horton, E. B., Folland, C. K., Alexander, L. V., Rowell, D. P., Kent, E. C., Kaplan, A., 2003. Global analyses of sea surface temperature, sea ice, and night marine air temperature since the late nineteenth century. *Journal of Geophysical Research-Atmospheres* 108, 4407, d14.
- Riihela, A., Mannien, T., Laine, V., 2013. Observed changes in the albedo of the Arctic sea-ice zone for the period 1982-2009. *Nature Climate Change* 3 (10), 895–898.
- Robinson, M., 2009. New quantitative evidence of extreme warmth in the Pliocene Arctic. *Stratigraphy* 6 (4), 265–275.

- Rybczynski, N., Gosse, J. C., Harington, C. R., Wogelius, R. A., Hidy, A. J., Buckley M., 2013 Mid-Pliocene warm-period deposits in the High Arctic yield insight into camel evolution. *Nature Communications* 4 (1550).
- Salzmann, U., Dolan, A., Haywood, A., Chan, W.-L., Voss, J., Hill, D., Abe-Ouchi, A., Otto-Bliesner, B., Bragg, F., Chandler, M., Contoux, C., Dowsett, H., Jost, A., Kamae, Y., Lohmann, G., Lunt, D., Pickering, S., Pound, M., Ramstein, G., Rosenbloom, N., Sohl, L., Stepanek, C., Ueda, H., Zhang, Z., 2013. Challenges in quantifying Pliocene terrestrial warming revealed by data-model discord. *Nature Climate Change* 3 (1), 969–974.
- Salzmann, U., Haywood, A., Lunt, D., Valdes, P., Hill, D., 2008. A new global biome reconstruction and data-model comparison for the Middle Pliocene. *Global Ecology and Biogeography* 17 (3), 432–447.
- Schreck, M., Meheust, M., Stein, R., Matthiessen, J., 2013. Response of marine palynomorphs to Neogene climate cooling in the Iceland Sea (ODP Hole 907A). *Marine Micropaleontology* 101, 49 – 67.
- Screen, J., Simmonds, I., 2010. Increasing fall-winter energy loss from the Arctic Ocean and its role in Arctic temperature amplification. *Geophysical Research Letters* 37.
- Seki, O., Foster, G. L., Schmidt, D. N., Mackensen, A., Kawamura, K., Pancost, R. D., 2010. Alkenone and boron-based Pliocene pCO<sub>2</sub> records. *Earth and Planetary Science Letters* 292 (1-2), 201–211.
- Semtner, A. J., 1976. A model for the thermodynamic growth of sea ice in numerical investigations of climate. *Journal of Physical Oceanography* 6, 379–389.
- Shu, Q., Song, Z., Qiao, F., 2015. Assessment of sea ice simulations in the cmip5 models. *The Cryosphere* 9 (1), 399–409.
- Wang, M., Overland, J., 2009. A sea ice free summer Arctic within 30 years? *Geophysical Research Letters* 36 (L07502).
- Zhang, J., Lindsay, R., Schweiger, A., Steele, M., 2013. The impact of an intense summer cyclone on 2012 Arctic sea ice retreat. *Geophysical Research Letters* 40 (4), 720–726.